Progress in Nuclear Energy 177 (2024) 105463

Contents lists available at ScienceDirect

Progress in Nuclear Energy

journal homepage: www.elsevier.com/locate/pnucene

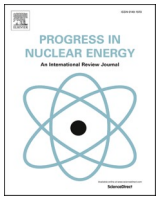

Radiation stability and durability of magnesium phosphate cement for radioactive reactive metals encapsulation

Fabio Fattori [a], Gabriele Magugliani [a,*], Andrea Santi [a], Eros Mossini [a], Ilaria Moschetti [a,b], Francesco Galluccio [a], Elena Macerata [a], Xavier de la Bernardie [b], Abdesselam Abdelouas [b], Davide Cori [c], Davide Comboni [d], Giacomo Diego Gatta [d], Mario Mariani [a]

[a] Politecnico di Milano, Department of Energy, Piazza Leonardo da Vinci, 32, 20133, Milano, Italy
[b] Subatech, CNRS/IN2P3, IMT Atlantique, Nantes University, BP 20722 cedex 3, Nantes, 44307, France
[c] Nucleco S.p.A., Via Anguillarese, 301, 00123, Roma, Italy
[d] Università degli Studi di Milano, Department of Earth Sciences, Via Sandro Botticelli, 23, 20133, Milano, Italy

ARTICLE INFO

Keywords:
Radioactive waste management
Radioactive reactive metallic waste
Magnesium phosphate cement
Gamma irradiation
Leaching
Radiation stability

ABSTRACT

The encapsulation of Radioactive Reactive Metallic Waste (RRMW) in ordinary Portland cement poses significant challenges due to its incompatibility with the alkaline environment of the matrix. To address this issue, magnesium phosphate cements (MPC) emerge as potential solutions for the safe and effective immobilisation of RRMWs. The radiation stability and durability of an optimised formulation have been examined for samples irradiated up to 1000 kGy, in particular concerning the leaching behaviour of the three main constituents of the cement hydration products, and on four artificially added elements used to simulate radionuclides commonly found in radioactive waste (caesium, strontium, europium, and cobalt). The mortars exhibited excellent leaching behaviour and a high mechanical resistance, even after irradiation, freeze-thaw cycles, and water immersion. No significant radiation-induced effects were observed in the mineralogical and microstructural properties of the mortars, thus supporting their stability at the examined doses. Having verified the compliance with the main Italian waste acceptance criteria, the results of this research represent an encouraging step for the future implementation of MPCs for RRMWs conditioning.

1. Introduction

Nuclear-related facilities are widely spread and serve various purposes, including energy production, research, medicine, and industrial applications, bringing significant benefits to humankind. For instance, Nuclear Power Plants (NPPs) are recognised as a reliable and effective source of clean energy due to their low emissions of CO_2 and other greenhouse gases (European Commission Joint Research Centre, 2021), (Nuclear Energy Agency, 2015). However, while nuclear technologies present several advantages, it is imperative to recognise and consider their associated critical aspects, particularly the safe management and disposal of Radioactive Waste (RW). Indeed, poor management practices in this regard can have detrimental effects not only in terms of human and environmental safety, but on the public acceptance of nuclear energy as well (Macfarlane, 2011), (Takada, 2022), (Choi, 2005). Nuclear waste management is a highly intricate process due to the wide range of forms, activities, and quantities in which the waste is generated, and it needs the implementation of multiple steps to effectively address such diverse waste characteristics (IAEA, 2022a), (IAEA, 2022b), (IAEA, 2017).

Any RW is referred to as *challenging* whenever further criticalities emerge in its management, such as high activity, difficult radiological characterisation, scarce knowledge—or even absence—of approved disposal routes, instability, or incompatibility with conditioning matrices due to intrinsic physico-chemical properties (INTERNATIONAL ATOMIC ENERGY AGENCY, 2007), (Electric Power Research Institute, 2006). A particularly important type of challenging RW is Radioactive Reactive Metallic Waste (RRMW), rich in neutron activation products hindering an effective characterisation (Bornhöft et al., 2023), (Robertson et al., 1990). In addition, encapsulation of RRMW poses safety concerns due to corrosion phenomena induced by waste-matrix interaction (Marsal, 2023). Indeed, conventional materials used for

* Corresponding author.
E-mail address: gabriele.magugliani@polimi.it (G. Magugliani).

https://doi.org/10.1016/j.pnucene.2024.105463
Received 22 July 2024; Received in revised form 19 September 2024; Accepted 24 September 2024
Available online 27 September 2024

the heterogeneous encapsulation of up to Intermediate Level Waste, namely formulations based on ordinary Portland cement (OPC), are unsuitable for RRMWs such as aluminium-, beryllium-, and tungsten-based alloys (Bart et al., 2013), (Covill et al., 2011). This is due to the alkaline nature of OPCs' pore water solution, which does not promote passivation of these metals as indicated by their Pourbaix diagrams (Deltombe and Pourbaix, 1958). Consequently, the absence of a stable outermost passivated layer results in continuous corrosion of the metal through interaction with free water, leading to the release of significant amounts of H_2 gas (Mendibide et al., 2021), (Caes et al., 2023). This phenomenon gives rise to detrimental long-term effects, including swelling, embrittlement, and premature cracking of the waste forms (Covill et al., 2011), (Mendibide et al., 2021), (Setiadi et al., 2006). Conversely, OPC-based formulations are instead fully compatible with stainless steels, since these alloys form a protective passive layer which is particularly dense and stable in alkaline environments (During, 2018).

Among the three mentioned metals, aluminium receives significant attention due to its widespread use in NPPs owing to its advantageous properties, including low thermal neutron capture cross-section and excellent mechanical and oxidation resistance (Kim et al., 2020). Beryllium is also employed in NPPs due to its high thermal conductivity and exceptional capability as neutron moderator and reflector (Hausner, 1963), (Beeston, 1971). In the forthcoming decades, with the advent of fusion power plants, it is predicted that substantial quantities of neutron-activated beryllium, along with tungsten, will be produced (Gonzalez de Vicente et al., 2022), (van der Laan et al., 2012). The proper encapsulation of these RRMWs is a crucial safety aspect to prevent radionuclide migration and ensure a durable waste form (Luhar, 2023). While surface-contaminated metals can undergo decontamination processes to reduce the volume of the waste, when dealing with bulk-activated metals it is generally more practical to directly condition the metal without specific treatments (Galluccio et al., 2021), (Rivonkar, 2022). In this latter case however, ensuring the compatibility between matrix and reactive metal becomes paramount.

To mitigate the corrosion of RRMWs and subsequent deterioration of the waste forms, one possible approach is to adopt other cementitious matrices which provide less alkaline pore solutions, creating an environment which falls within the passivation region of these metals. This would allow for the formation of a stable metal oxide protective layer, preventing further reactions. Magnesium Phosphate Cement (MPC) formulations are promising solutions to this problem. MPCs are produced through an acid-base reaction involving an acid water-soluble phosphate salt, low-reactivity—either hardburnt or dead-burnt—magnesium oxide (MgO), and water (Haque and Chen, 2019). Common phosphate salts employed in MPCs are potassium dihydrogen phosphate (KDP) and, in the past, ammonium dihydrogen phosphate (ADP) (Fan and Chen, 2014). When using KDP, the main resulting hydration product, known as K-struvite ($MgKPO_4 \bullet 6H_2O$), effectively bonds the unreacted MgO grains together, developing strength in the paste (Ojovan and Lee, 2014), (Lahalle et al., 2016), (Le Rouzic et al., 2017).

In other applications, such as concrete restoring or construction, the very short setting time of MPCs is undoubtedly a desirable feature (Haque and Chen, 2019), (Li and Chen, 2013). However, when it comes to radioactive waste management, it is vital to delay the setting to ensure proper mortar homogenisation and waste encapsulation. To achieve this, set retarders such as borax [$Na_2(B_4O_5)(OH)_4 \cdot 8H_2O$], boric acid ($H_3BO_3$), or less commonly sodium triphosphate ($Na_5P_3O_{10}$) have been evaluated. Currently, the use of borate-based compounds has become a standard choice due to their effectiveness (Fan and Chen, 2014), (Hall et al., 2001), (Walling and Provis, 2016). Furthermore, over the past years, the investigation of sustainable matrices for RW conditioning has been particularly investigated, and there is a strong desire to continue focusing on this approach (Saleh et al., 2022), (Eskander et al., 2012), (Saleh and Eskander, 2013), (Santi et al., 2022). Also for this reason, environmentally friendly inert filler materials like sand, blast furnace slag, volcanic ash, or metakaolin are often incorporated to improve mechanical properties and reduce costs, while the addition of fly ash, an industrial by-product, further enhances the workability of the mortar (Qin et al., 2020), (Gardner et al., 2015), (Akroyd and AKROYD, 1962), (Saha, 2018). Numerous studies have already demonstrated the suitability of this matrix for the encapsulation of RRMWs, alongside its favourable properties, such as elevated mechanical resistance, rapid strength development, low permeability, and reduced water consumption (Covill et al., 2011), (Bykov et al., 2022), (Pyo et al., 2021), (Chartier et al., 2020), (Bykov et al., 2020), (Moschetti et al., 2023), (Fang, 2023).

In this study, conducted within EU's H2020-PREDIS (PRE-DISposal management of radioactive waste) project, a meticulous investigation was undertaken to evaluate the radiation stability and durability of the formulation proposed by Chartier et al. (2020). A comprehensive examination of samples exposed to radiation doses up to 1000 kGy was carried out to test the performance of the formulation, in particular in terms of leaching resistance. Moreover, the leaching behaviour of four noteworthy contaminants was investigated by adding them to the fresh mortar. Caesium and strontium, representatives of common fission products Cs-137 and Sr-90, were included to understand the behaviour of 1st and 2nd group elements. Europium, a lanthanide representative, was included since some of its isotopes, such as Eu-152 and Eu-154, are fission and activation products. Lastly, cobalt acts as transition metal representative, also mimicking the activation product Co-60 commonly found in irradiated metallic alloys. The obtained results were juxtaposed with those derived from non-irradiated reference samples for a comparative analysis. Furthermore, to enhance comprehension and validate the experimental evidence, supplementary characterisation tests were conducted via powder X-Ray Diffraction (XRD), micro-Computed Tomography (micro-CT), and Scanning Electron Microscopy (SEM). Ultimately, compression tests were carried out on samples which underwent different ageing procedures, including gamma irradiation, water immersion, and freeze-thaw cycles, to ascertain compliance with the Waste Acceptance Criteria (WAC) set by the Italian regulatory body.

2. Materials and methods

2.1. Raw materials

The specimens of MPC were prepared using hardburnt MgO (MAGCHEM 10CR, Martin Marietta Magnesia Specialties) and low cost KDP (YARA). Boric acid (VWR Chemicals BDH) was chosen as set retarder. All the employed reagents had a high grade of purity, at least 98%.

The quartz-rich sand, with high content of silicon dioxide ($SiO_2 >$ 99%), was supplied by Sibelco corporate (particle size distribution 0.1–1.2 mm, $d_{50} = 483$ μm). The class F fly ash came from the Électricité de France coal power plant of Cordemais, France; its characterisation by means of Energy Dispersive X-ray Fluorescence (ED-XRF) reported as main constituents SiO_2 (53% wt.), Al_2O_3 (20% wt.), Fe_2O_3 (11% wt.), and CaO (6% wt.).

2.2. Samples preparation and curing

For the preparation of the MPC-based mortar, a planetary mixer was employed in accordance with the European standard EN 196–1:2016 (Ente italiano di normazione, 2016). Following a vigorous pre-mixing, weighed amounts of the dry powders (sand, fly ash, magnesia, and KDP) were gradually added to the water and boric acid solution. The formulation, reported in Table 1, imposed a Mg/P theoretical molar ratio of 1 mol/mol and a water-to-cement ratio of 0.51 g/g. A mixing time of approximately 5 min is required to achieve a homogeneous grout. The resulting mortar had good workability and an initial setting time of approximately 20 min, as expected (Chartier et al., 2020).

Table 1
MPC formulation for 1 L of mortar (Chartier et al., 2020).

Material	Mass (g)
MgO	131.39
KH_2PO_4	443.58
Sand	574.97
Fly ash	574.97
H_3BO_3	11.50
Water	293.24

Mortars were cast in equilateral cylinders of 5 cm; to grant comparability, all the samples employed in this study were cast from the same mortar batch. All samples were demoulded after 24 h and subsequently cured in a climatic chamber for 28 days in water-saturated environment (relative humidity greater than 90%) under controlled temperature (22 ± 1 °C).

The water and boric acid solution was prepared by mixing the quantities reported in Table 1. Stable isotopes of the contaminants were added to the same solution as analytical-grade salts: $CsNO_3$ (Sigma-Aldrich), $Co(NO_3)_2 \cdot 6\ H_2O$ (Sigma-Aldrich), $Eu(NO_3)_3 \cdot 6\ H_2O$ (Fluka), and $Sr(NO_3)_2$ (Sigma-Aldrich). No precipitates were observed due to the high solubility of the species. The concentration of the cations was analysed via ICP-MS, and the resulting concentration in the fresh mortar is reported in Table 2.

2.3. Gamma irradiation

In order to mimic the long-term radiation damage experienced by real waste forms due to the presence of radioactive material, some samples were irradiated with an industrial Co-60 irradiator selecting cumulative absorbed doses of 200, 500, and 1000 kGy delivered at a constant dose rate of 2.5 kGy/h. For reference, some samples were kept unirradiated and tested after the same ageing period of the irradiated ones.

2.4. Leaching tests

The three-dimensional leaching tests were conducted based on the ANSI/ANS-16.1-2019 protocol (American National Standards Institute, 2019). The leaching process involved samples irradiated at 200, 500, and 1000 kGy, plus a non-irradiated blank sample, for a total time of three months in osmotic water at constant temperature (22 ± 1 °C) divided into twelve different intervals. The purpose of a semi-dynamic leaching test is to study the behaviour of certain elements in controlled and accelerated conditions, to simulate their release over a timeframe of approximately one hundred years. The analytes of interest are the main constitutive elements of the matrix, namely magnesium, phosphorus, and potassium, as well as the four contaminants. The leachability index L is globally used by regulatory bodies to assess the leaching behaviour of the conditioned waste forms and establish appropriate WAC. According to the standard, the leachability index for a given element i is defined as:

$$L_i = \log\left(\frac{\beta}{D_{e,i}}\right) \tag{1}$$

where β is a defined constant (1.0 cm^2/s), and $D_{e,i}$ (cm^2/s) is the effective diffusivity of the element i. The latter is calculated under the hypothesis of a semi-infinite solid model as:

$$D_{e,i} = \frac{\pi}{4} m_i^2 \tag{2}$$

m_i being the slope of the linear regression equation of the quantity $y_{i,k}$ for an element i up to the k-th time interval, as a function of the square root of the cumulative time. $y_{i,k}$ is calculated as follows:

$$y_{i,k} = CF_{i,k} \cdot \frac{V}{SA} \tag{3}$$

where $CF_{i,k}$ is the cumulative released fraction of the element i up to the k-th time interval, while V and SA are the volume (cm^3) and surface area (cm^2) of the specimen, respectively. In agreement with the ANSI/ANS-16.1-2019 protocol (American National Standards Institute, 2019), data from the first four days of leaching were employed to derive the leachability indices according to Equation (1).

The normalised leaching rate (NLR) can also be calculated as:

$$NLR_{i,n} = \frac{a_{n,i}}{SA \cdot t_n} \tag{4}$$

where $a_{n,i}$ represents the leached quantity of a given element i in the n-th interval in terms of mass, and t_n is the leaching time at the interval n.

Leaching tests were carried out over a time of 90 days to simulate the release over long time intervals, and the corresponding cumulative released fractions for each element were derived. Considering all the aforementioned pieces of information, a thorough and accurate breakdown of the samples' leaching behaviour can be achieved.

2.4.1. Analyses of the leachates

Elemental analysis techniques were adopted to determine the leached fractions of the abovementioned matrix constituents and contaminants. Inductively Coupled Plasma-Optical Emission Spectroscopy (ICP-OES, Avio 500, PerkinElmer) was utilised to measure the concentration of constitutive matrix elements within each leachant sample. Inductively Coupled Plasma-Mass Spectrometry (ICP-MS, NexION, 2000; PerkinElmer) was instead employed for the identification of leached contaminants thanks to its lower detection limit. At the end of the respective test interval, all leachate samples were acidified using a 67% wt. ultrapure HNO_3 solution and duly diluted afterwards for analysis using a 1% wt. ultrapure HNO_3 solution, consistently with previous works (Santi et al., 2022), (Mossini, 2023). ICP-OES and ICP-MS were calibrated employing properly diluted Inorganic Ventures CMS-x standard solutions.

Table 2
Concentration of the four contaminants present in the cement paste.

Element	Concentration [ppm[a]]
Cobalt	56.8 ± 0.3
Strontium	671.3 ± 9.1
Caesium	474.3 ± 7.8
Europium	402.7 ± 4.3

[a] ppm: parts per million, to be intended as a mass fraction.

2.5. Compressive strength tests

The compressive tests were conducted following the EN 12390–3:2019 procedure (Ente italiano di normazione, 2016). The results are expressed as the ratio between the maximum sustained load and the upper surface area of the sample and reported in MPa.

In order to mimic the damage caused to the waste forms by accidental flooding of the repository, both irradiated and non-irradiated samples were tested for compressive strength after the 90-day leaching period. The results were then compared to non-leached specimens to further evaluate possible effects on the matrices in terms of durability. The Italian WAC require a minimum value for the compressive strength at 28 days of curing and after 90 days of immersion of 10 MPa (Ispettorato Nazionale per la Sicurezza Nucleare e la Radioprotezione, 2023).

2.6. Freeze-thaw cycles

The freeze-thaw cycles were conducted following the UNI 11193-2006 protocol (Ente italiano di normazione, 2006), after which a compression test was carried out. These tests were performed to simulate the possible detrimental effects caused by seasonal and daily thermal excursions, including freezing which may impact on the pore water solution. In accordance with the Italian requirements, a minimum compressive strength of 10 MPa is required after 30 cycles on non-irradiated samples. Each cycle involves temperature variations from −40 °C to +40 °C, over a 24-h period, with minimum ramps of 10 °C/h between the extremes (Saha, 2018).

2.7. Sample characterisation

Powder X-ray diffraction (XRD) was carried out at the Earth Sciences Department A. Desio, University of Milan, with an automated Panalytical X'Pert Pro modular diffractometer, equipped with a X'Celerator detector and with the following operating conditions: 2ϑ range from 4° to 80° and step size of 0.017°, monochromatized Cu-Kα radiation, 40 kV, 40 mA, counting time of 240 s per step, top-loaded samples. Phase identification was performed using the X'Pert HighScore suite and database. Obtained patterns were processed and plotted using MATLAB software suite.

The micro-computed tomography (micro-CT) was performed with an Easy Tom XL/RX Solutions instrument, using a tungsten X-ray source with 100 kV and 100 μA settings, a 1 mm aluminum high-pass filter, and a Charge-Coupled Device camera with a resolution of 1516x1920 pixels. Micro-CT imaging produced a 3D distribution of attenuation coefficients (μ) that are related to mass density (ρ) of the analysed material. After using the Xact program to reconstruct the 3D attenuation dataset, the resulting volume was presented in three dimensions and post-processed with the Dragonfly 2020.2 software (Object Research System Inc. Montreal, Canada, 2020) enabling a multi-directional study of the specimens. Once the volumes of interest were selected, it was possible to isolate the pores from the rest of the MPC matrix by selecting only specific density values. Information about the pores was obtained, such as:

- the volume of each pore, through which the porosity of the samples was calculated as the ratio between the total pores volume and the volume of interest;
- the pore characteristic dimensions, allowing to assess the pore size distribution and the cumulative porosity curve.

Scanning Electron Microscopy (SEM) was performed using a JEOL JSM-5800LV microscope operating at 15 kV. Quantitative elemental mappings with Energy-Dispersive X-ray spectroscopy (EDX) were performed with a SAMx (NumeriX+) energy-dispersive spectrometer mounted on the SEM. The samples were firstly impregnated with epoxy resin and then polished. Prior to analysis, a 40 nm layer of carbon was deposited on the surface of the samples to ensure good conductivity. For each sample, two areas of 120 × 150 μm^2 were investigated.

3. Results and discussion

3.1. Macroscopic examination of irradiated and leached samples

All the irradiated specimens underwent a preliminary visual inspection revealing no evidence of degradation, such as fractures, cracks, or chips. This observation holds true for cumulative absorbed doses of up to the maximum considered value, i.e. 1000 kGy, as illustrated in Fig. 1. Additionally, no macroscopic signs of swelling or shrinkage were detected. Visual inspection of the leached samples also confirmed the absence of macroscopic alterations or damage during the leaching period.

3.2. Leaching behaviour of irradiated samples

3.2.1. Main constituents

The cumulative release curve of K after 4 days of leaching is shown in Fig. 2. The high released fraction of potassium is to be expected due to its high concentration in the pore solution in comparison to the other elements (Lahalle et al., 2019). Following an initial transient, a diffusion-driven mechanism is prevalent in which ions migrate by longer pathways from the bulk of the MPC samples, resulting in a reduced release rate (Elkamash et al., 2006). Overall, the theoretical diffusion-driven behaviour is respected, although it is important to remark that these results must be taken cautiously since mass transfer inside cementitious materials is complicated by a plethora of processes occurring simultaneously, thus diffusion is still extremely difficult to predict inside these matrices (Hinsenveld, 1991), (Godbee and Joy, 1974). Similar reasonings can be made regarding magnesium and phosphorus. All samples exhibited comparable cumulative releases after 90 days of test, irrespectively of the absorbed dose; values in the order of 16 ± 1%, 7 ± 0.5%, and 2 ± 0.5% were measured for potassium, phosphorus, and magnesium, respectively.

The calculated leachability indices are reported in Table 3. No significant radiation-induced changes can be inferred since all the samples

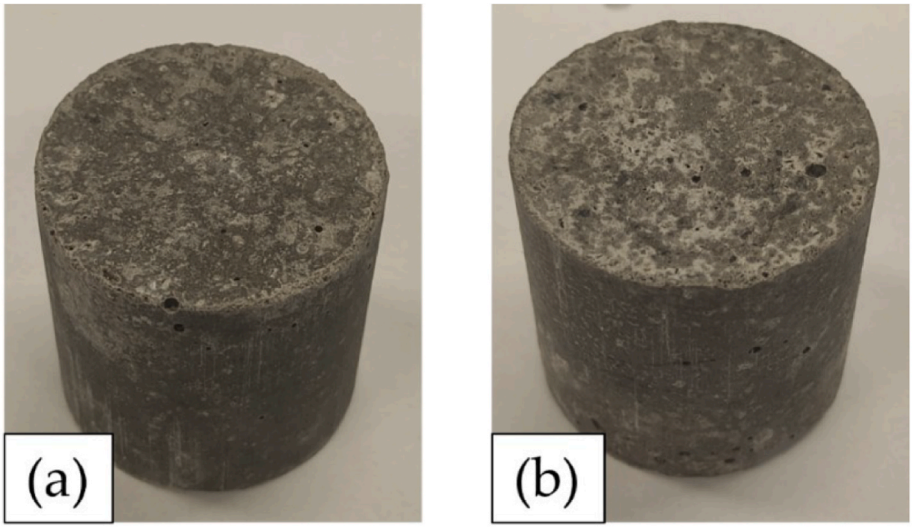

Fig. 1. MPC samples (a) not irradiated (b) irradiated, cumulative dose of 1000 kGy.

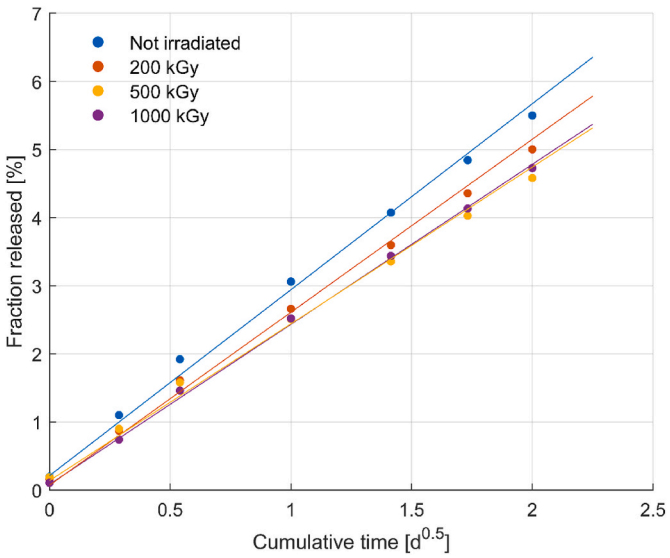

Fig. 2. Potassium cumulative release curve for the first four days of leaching; uncertainty bars are within marker size.

Table 3
Leachability indices of the main matrix constituents.

Dose	Element		
	Mg	K	P
Not irradiated	9.6 ± 0.2	8.4 ± 0.1	8.9 ± 0.1
200 kGy	9.4 ± 0.2	8.5 ± 0.1	8.9 ± 0.1
500 kGy	9.4 ± 0.1	8.6 ± 0.1	9.0 ± 0.1
1000 kGy	10.1 ± 0.1	8.5 ± 0.1	9.2 ± 0.1

exhibited comparable values when related to the non-irradiated blank sample, irrespectively of the absorbed dose. Stability of the MPC matrix in terms of leaching resistance for absorbed doses up to 1000 kGy is therefore suggested, further confirming literature outcomes (Chartier et al., 2020), (Bykov et al., 2020).

3.2.2. *Contaminants*

The leachability indices of the four contaminants investigated are displayed in Fig. 3.

The leachability indices of europium are consistent with the non-irradiated sample, taken as reference, but lower than those reported for OPCs in similar experimental configurations (Goo et al., 2021). This lower performance is attributed to the low solubility of lanthanides in alkaline environments, meaning that Eu may be more easily released from MPCs than from OPCs (Abdelrahman et al., 2007). However, considering the very high leachability indices, this difference may be of limited significance. Despite belonging to different chemical groups, cobalt and strontium exhibited similar leaching behaviours. Furthermore, the leachability indices of both contaminants remained comparable across different absorbed doses, supporting the hypothesis that irradiation had minimal influence. The results obtained for cobalt are slightly worse than those typically reported for OPC matrices (Goo et al., 2021), (Shon et al., 2019), (Shon et al., 2022). Also in this case, this can be explained due to the higher pH of the OPC pore solution compared to that of MPC since highly alkaline environments favour metal precipitation and consequently hinder diffusion and dissolution in the leachant (INTERNATIONAL ATOMIC ENERGY AGENCY, 1992). Regarding strontium, the leachability indices of the irradiated samples are instead consistent with those reported in the literature for OPC and other MPC formulations (Pyo et al., 2021), (Goo et al., 2021), (Shon et al., 2019), (Shon et al., 2022), (Vinokurov et al., 2009).

Caesium exhibited the poorest leaching behaviour, which is expected considering its high mobility and solubility. Its release is nevertheless in accordance with the theoretical model trend already discussed for the matrix constituents. Fig. 4 shows the caesium cumulative release curve after 4 days of leaching and might suggests a radiation-induced effect in the leaching behaviour, as the non-irradiated reference sample has a lower release compared to the other samples, in the order of some percentage points. Nevertheless, this worsening is negligible when considering the leachability indices and associated uncertainties. As depicted in Fig. 3, comparable leachability indices are in fact obtained across all samples regardless of the absorbed dose. The normalised leaching rates of caesium, shown in Fig. 5, exhibit a consistent decrease over time for all specimens. This trend suggests that during the instantaneous surface dissolution phase the predominant release of caesium can be attributed to non-immobilised atoms (Ojovan and Lee, 2014). After approximately 7 days, it is already possible to infer that a significant portion of the residual caesium has been immobilised. Furthermore, the values are similar to those reported for OPC matrices (Ojovan et al., 2011). The successful encapsulation of caesium may be attributed to its incorporation within the MPC paste, possibly resulting in the formation of a struvite-(K,Cs), as reported by Wagh et al., which is not

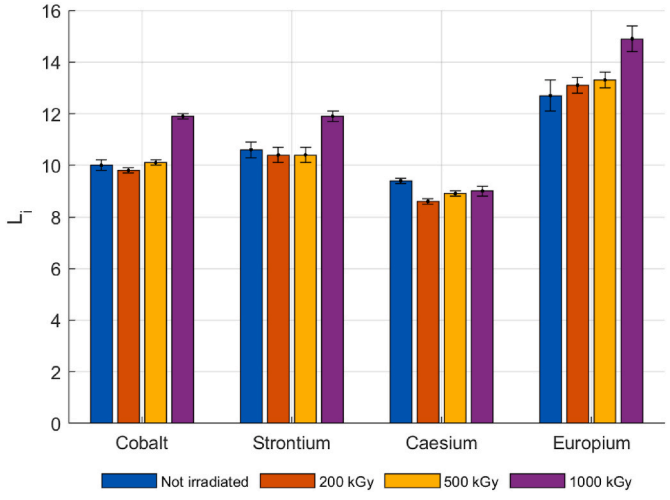

Fig. 3. Variation in leachability indices of the contaminants with absorbed dose.

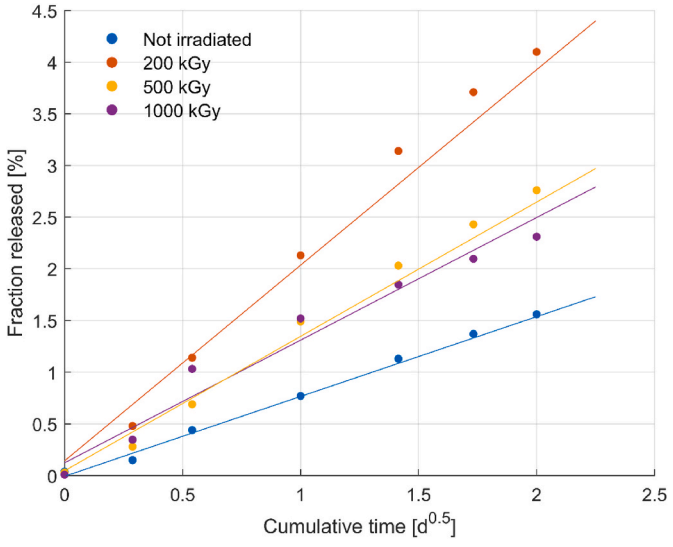

Fig. 4. Caesium cumulative leaching curves for the first four days of leaching; uncertainty bars are within marker size.

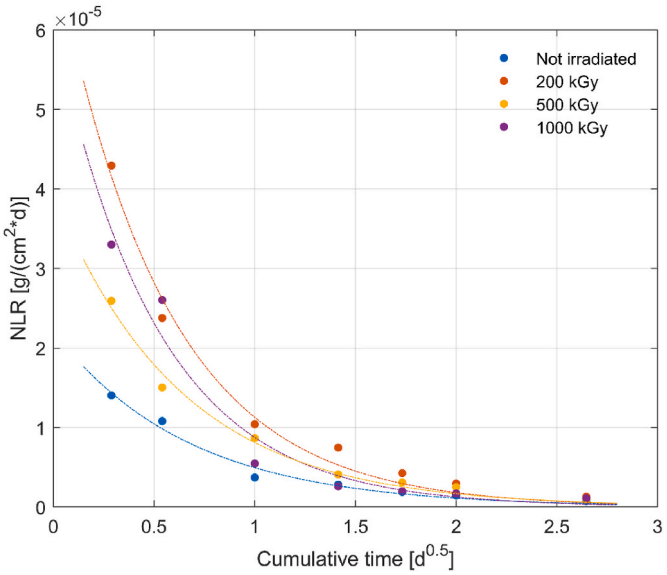

Fig. 5. Caesium normalised leaching rates for the first seven days of leaching; uncertainty bars are within marker size.

water-leachable and effectively hinders its dispersion (Wagh, 2016). However, no experimental evidence of struvite-(K,Cs) was observed in this work, probably due to the low concentrations of caesium in the fresh mortars.

Additional insight into the leaching behaviour of the contaminants can be obtained by reporting their cumulative releases after a 90-day leaching period. Similar long-term release values were obtained, in the order of 5 ± 1% for caesium, 1 ± 0.5% for cobalt, 0.8 ± 0.6% for strontium, and 0.1 ± 0.05% for europium. It is worth mentioning that such a cumulative release of caesium over a three-month leaching period is a favourable outcome. In fact, these results are comparable to, or even lower than, those observed in other OPC-based matrices (Goo et al., 2021), (Abdelrahman et al., 2007), (Shon et al., 2019), (Shon et al., 2022), further supporting the hypothesised formation of a poorly soluble struvite-(K,Cs) phase.

3.3. Mechanical strength

All MPC specimens subjected to 90 days of leaching in osmotic water underwent monoaxial compression and the results were compared to the corresponding non-leached reference samples across all investigated doses. The results are presented in Table 4, in compliance with the Italian WAC requirement (10 MPa) with encouraging safety margin, indicating a promising mechanical performance of this MPC matrix against leaching and irradiation up to 1000 kGy. These findings align with previous studies on other MPC formulations (Li and Chen, 2013), (Park et al., 2016), (Wang et al., 2022), (Yu et al., 2021). All irradiated samples showed compression strengths comparable to the non-irradiated references, as already reported in literature (Chartier et al., 2020). Moreover, it is worth emphasising that at least 70% of the initial strength was retained after a 90-day leaching, a result comparable to that observed in OPCs (Shon et al., 2019), (Shon et al., 2022), (Cheng et al., 2013).

Table 4
Compression strength before and after leaching of different samples.

Dose	Not leached [MPa]	Leached [MPa]
Not irradiated	39.7 ± 4.0	30.7 ± 3.1
200 kGy	40.1 ± 4.0	28.1 ± 2.8
500 kGy	37.1 ± 3.7	28.9 ± 3.0
1000 kGy	35.8 ± 3.6	30.3 ± 3.0

3.4. Freeze-thaw cycles

Following freeze-thaw cycles, non-irradiated MPC samples underwent monoaxial compression and were compared to reference samples having the same age. The compression test outcomes were 36.3 ± 5.4 MPa for the control sample and 31.7 ± 4.8 MPa for the specimen subjected to thermal cycles, with an overall loss of about 12%. This slight worsening can be explained by the expansion of the pore solution upon freezing, giving rise to higher internal hydraulic pressure which can cause deterioration of the matrix (Cai and Liu, 1998). Additionally, thermal stresses arising from these cycles could build up, causing changes in the structure and further deterioration (Penttala and Al-Neshawy, 2002), (Guo et al., 2022). These results are to be considered positive and comparable to those obtained for typical OPC formulations (Arasteh-Khoshbin et al., 2023). Furthermore, the Italian WAC of at least 10 MPa is respected with a reasonable safety margin.

3.5. Characterisation of samples

3.5.1. Mineralogical and phase analysis

The powder XRD patterns of the different samples were acquired to investigate the phase compositions. The spotlight was put on irradiated, both leached and non-leached, specimens in comparison with the non-irradiated ones.

Fig. 6 compares the four extreme scenarios regarding leaching and irradiation, i.e. 1000 kGy. Aside for small intensity differences, most likely ascribable to the effect of modest preferred-orientation of the crystallites, the resulting patterns are virtually identical, with K-struvite and quartz as dominant crystalline phases. The detection of mullite and sillimanite, as subordinate phases, is likely due to the presence of fly ash inside the matrix. As the periclase principal Bragg peaks are almost overlapped with those of mullite (at *ca.* 36.9° and 42.9° 2θ, with Cu-*K*α radiation), the presence of a minor fraction of unreacted MgO cannot be ascertained. Overall, no significant differences are noticeable among samples, thus the stability of the mineralogical phases under leaching and irradiation can be inferred.

3.5.2. Micro-CT analyses

The micro-CT was carried out to investigate the morphology of the samples through a non-destructive technique. The choice of the specimens to be analysed was the same as reported in section 3.5.1. Fig. 7 shows a slice representation of the four samples. Considering the grey scale representation, it is possible to associate the black areas to pores,

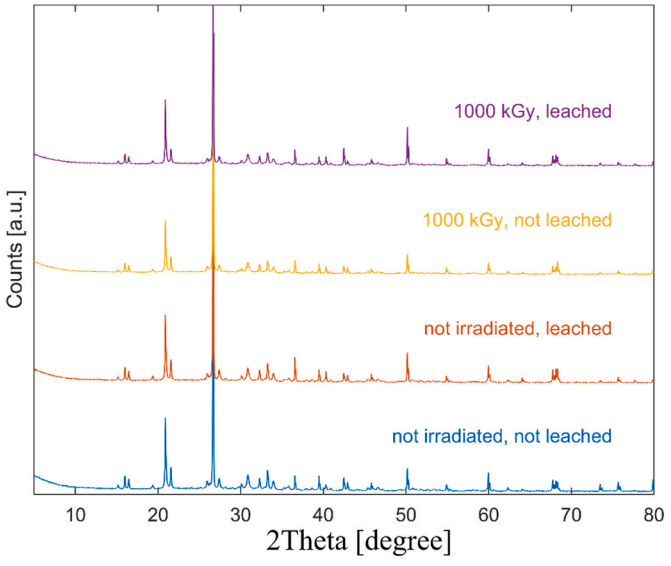

Fig. 6. Powder XRD patterns of different samples.

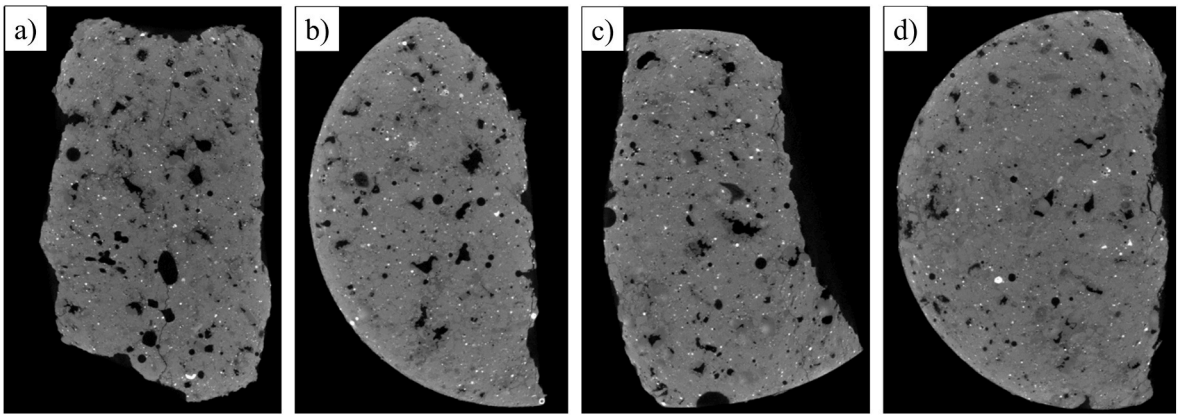

Fig. 7. Micro-CT slice images of the four samples: a) not irradiated; not leached b); not irradiated, leached; c) 1000 kGy, not leached; d) 1000 kGy, leached.

cracks, and voids. No significant differences can be inferred to either leaching or irradiation on a macroscopic level.

The samples were further analysed to determine variations on a microscopic level, namely in terms of porosity. The results, reported in Table 5, are comparable to those found in other MPC literature works for similar pore diameter ranges, i.e. above few micrometres (Lahalle et al., 2019), (Xu et al., 2017). Both irradiation and leaching seemed to have a positive influence in terms of porosity of the samples. However, this outcome disagrees with findings from other leaching and irradiation studies on cementitious matrices, in which a porosity increase was observed (Khmurovska et al., 2021), (Ekström, 2001).

Looking at the pore size distribution in Fig. 8, which includes characteristic dimensions in the range 10–100 μm, the distributions are almost identical. Furthermore, considering the cumulative porosity curves in Fig. 9, it can be confirmed that the total porosity is not significantly affected by leaching or irradiation conditions in the considered pore size range. Greater differences emerge when considering pore sizes larger than 100 μm which fall in the typical range of coarse pores, such as air voids linked to mixing or specimen preparation (Thomson et al., 2007), (Hover, 2011). However, alteration of smaller sized pores, down to few nanometres, may be caused by leaching or irradiation.

3.5.3. SEM-EDX analyses

SEM-EDX characterisation was performed to investigate the composition of the samples. The choice of the specimens to be analysed was the same as reported in section 3.5.1. In each analysed sample, a scan was performed according to the characteristic elements (Al, K, Mg, P, and Si) to find remarkable spots for further investigation. Several crystallites were scanned with EDX to highlight possible differences in the elemental composition of K-Struvite. Fig. 10 shows the obtained SEM images, in which zones of interest indicating the presence K-struvite, fly ash, and silica were highlighted.

The areas rich in K-struvite were further analysed by EDX to estimate

Table 5
Porosity evaluation of different samples.

Dose	Volume of interest (mm^3)	Total pores volume (mm^3)	Maximum pore volume (mm^3)	Porosity (%)
Not irradiated, not leached	118.02	8.88	1.45	7.52
Not irradiated, leached	85.17	6.01	1.17	7.06
1000 kGy, not leached	239.46	13.07	0.87	5.46
1000 kGy, leached	313.02	15.10	1.33	4.82

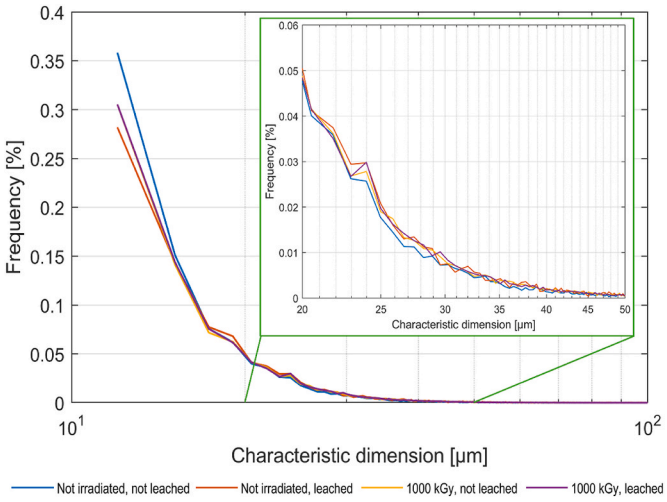

Fig. 8. Pore size distributions of the four samples in the range 10–100 μm.

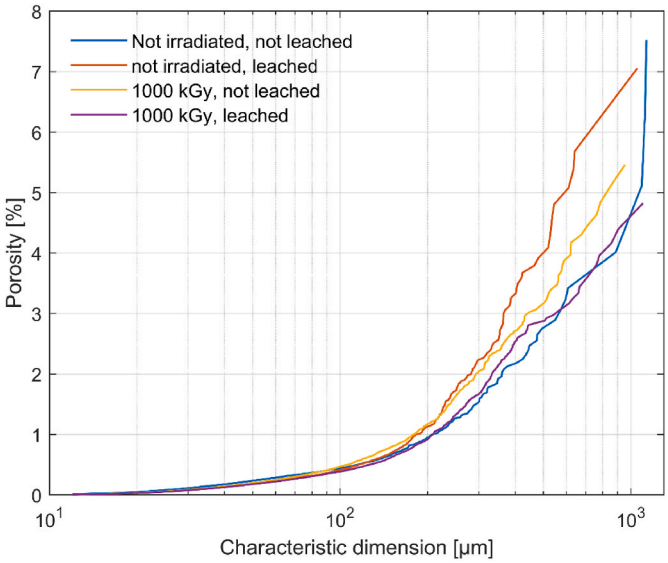

Fig. 9. Cumulative porosity curves of the four samples in the range 10–1000 μm.

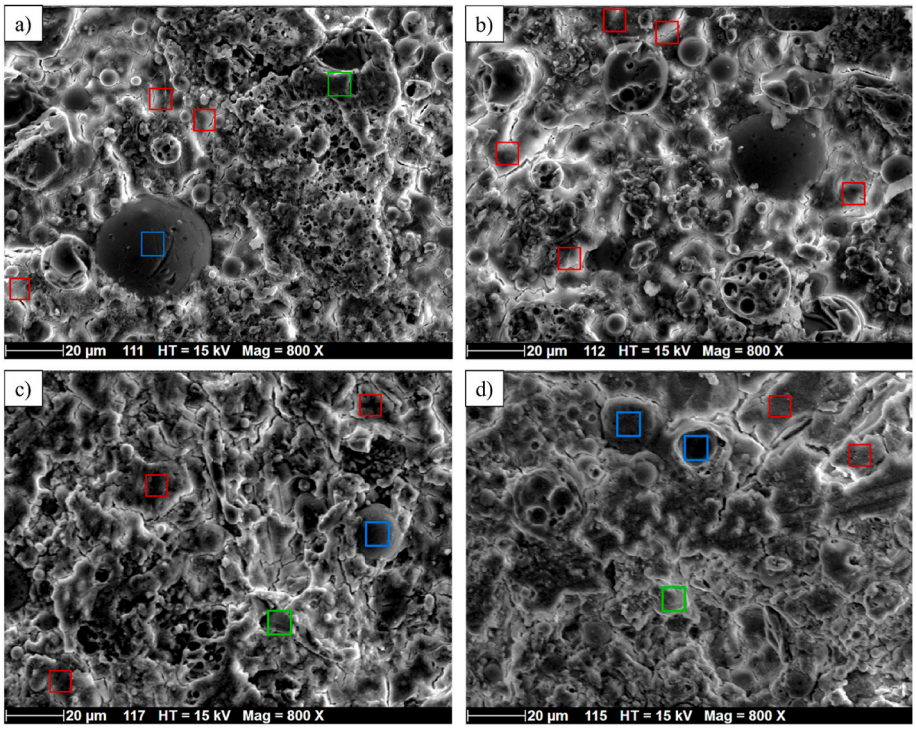

Fig. 10. SEM images of MPC samples: a) not irradiated, not leached; b) not irradiated, leached; c) 1000 kGy, not leached; d) 1000 kGy, leached. Spots in red squares were analysed by EDX and are representative of K-struvite, while the blue and green ones are fly ash and silica, respectively.

Table 6
Minimum and maximum values of the molar ratios of the main K-struvite components; SD is the standard deviation.

Sample	Mg/P (mol/mol)			Mg/K (mol/mol)			K/P (mol/mol)		
	MIN	MAX	SD	MIN	MAX	SD	MIN	MAX	SD
Not irradiated, not leached	0.69	0.97	0.12	0.78	1.35	0.21	0.70	0.93	0.09
Not irradiated, leached	0.68	1.11	0.15	0.76	1.80	0.37	0.62	0.88	0.10
1000 kGy, not leached	0.75	1.16	0.15	1.01	1.44	0.16	0.72	0.81	0.06
1000 kGy, leached	0.66	0.96	0.11	0.74	1.32	0.21	0.72	0.90	0.06

molar ratios of the three main components of K-struvite, namely Mg, K, and P. The results, reported in Table 6, are mostly lower than the theoretical stoichiometric value of 1 mol/mol expected for this MPC formulation. The ratio with the highest standard deviation is for Mg/K. Similar results were found in a work by Lahalle et al. (2019), in which the high uncertainty was associated to a difference in the morphology of the K-struvite (needle or continuous matrix). As shown in Fig. 10, there is no change in morphology at the various points considered. The difference may therefore be due to some precipitation of a different phase or the incomplete dissolution of KH_2PO_4. However, no significant differences can be observed following immersion and/or irradiation, once again suggesting the stability of the mineralogical phases and the durability of this MPC formulation.

4. Conclusions

MPC mortars exhibit promising resistance towards high doses of gamma radiation—up to at least 1000 kGy—with no quantifiable worsening in the compressive strength and leaching behaviour, nor changes in mineralogy or morphology when compared to non-irradiated reference specimens. Additionally, the corresponding Italian WAC are respected for each sample with a reliable margin above the lower limit, also when considering the resistance to freeze-thaw cycles. The immobilisation of caesium and cobalt, both strong beta/gamma emitters, is particularly important. The mobility of Cs-137 and the abundance of Co-60 in metal alloys make their successful containment significant accomplishments in terms of radioactive waste management. Furthermore, the successful encapsulation of strontium and europium radionuclides is also noteworthy, as they are common fission and activation products from different chemical groups. Their proper confinement contributes to the overall effectiveness of the waste immobilisation process.

As a consequence of the mentioned evidence, the investigated MPC formulation is a potential candidate for the conditioning of RRMW. Nevertheless, further studies are necessary to confirm the preliminary results obtained in this work. Additional efforts will be made to evaluate the leaching behaviour of different contaminants, in particular actinides, and new tests will be performed to assess full compliance with WACs. The durability of the matrix will undergo additional evaluation through freeze-thaw cycles applied to specimens irradiated up to 1000 kGy. Moreover, forms should be synthesized with surrogate and real waste for the representativeness of the analysis.

CRediT authorship contribution statement

Fabio Fattori: Writing – original draft, Visualization, Investigation, Data curation, Conceptualization. **Gabriele Magugliani:** Writing – review & editing, Data curation. **Andrea Santi:** Writing – review & editing, Supervision, Conceptualization. **Eros Mossini:** Writing – review & editing, Supervision, Funding acquisition, Conceptualization. **Ilaria**

Moschetti: Writing – review & editing, Visualization, Investigation, Data curation. **Francesco Galluccio:** Writing – review & editing. **Elena Macerata:** Writing – review & editing. **Xavier de la Bernardie:** Investigation, Data curation. **Abdesselam Abdelouas:** Project administration. **Davide Cori:** Investigation, Data curation. **Davide Comboni:** Writing – review & editing, Investigation, Data curation. **Giacomo Diego Gatta:** Writing – review & editing, Investigation, Data curation. **Mario Mariani:** Project administration.

Declaration of competing interest

The authors declare that they have no known competing financial interests or personal relationships that could have appeared to influence the work reported in this paper.

Data availability

Data will be made available on request.

Acknowledgements

This work was conducted within EU H2020-PREDIS project, which has received funding support from the Euratom research and training program 2019–2020 under grant agreement No. 945098. The authors thank Gammatom S.r.l. for their irradiation facility and PLASSMAT platform at IMN (Nantes, FR) for their SEM-EDX measurement equipment.

References

Abdelrahman, R., Zaki, A., Elkamash, A., 2007. Modeling the long-term leaching behavior of 137Cs, 60Co, and 152,154Eu radionuclides from cement–clay matrices. J. Hazard Mater. 145 (3), 372–380. https://doi.org/10.1016/j.jhazmat.2006.11.030. Jul.

Akroyd, T., 1962. Chapter 1 - The properties of concrete. In: AKROYD, T.N.W. (Ed.), Concrete: Properties and Manufacture. Pergamon, pp. 1–45. https://doi.org/10.1016/B978-0-08-009595-0.50004-5.

American National Standards Institute, 2019. Measurement Of The Leachability Of Solidified Low-Level Radioactive Wastes By A Short-Term Test Procedure (ANSI/ANS-16.1-2019). Feb. 22,.

Arasteh-Khoshbin, O., Seyedpour, S.M., Brodbeck, M., Lambers, L., Ricken, T., 2023. On effects of freezing and thawing cycles of concrete containing nano-SiO_2: experimental study of material properties and crack simulation. Sci. Rep. 13 (1), 22278. https://doi.org/10.1038/s41598-023-48211-4. Dec.

Bart, F., Cau-di-Coumes, C., Frizon, F., Lorente, S., 2013. Cement-Based Materials for Nuclear Waste Storage. Springer New York, New York, NY. https://doi.org/10.1007/978-1-4614-3445-0.

Beeston, J.M., 1971. Beryllium metal as a neutron moderator and reflector material. Nucl. Eng. Des. 14 (3), 445–474. https://doi.org/10.1016/0029-5493(70)90161-5. Feb.

Bornhöft, M., et al., 2023. Deliverable 9.7: ROUTES -Review of radioanalytical characterisation of selected radioactive wastes and wastes with complex chemical and toxic properties.

Bykov, G.L., Ershov, V.A., Ershov, B.G., 2020. Radiolysis of the magnesium phosphate cement on γ-irradiation. Constr Build Mater 252, 119156. https://doi.org/10.1016/j.conbuildmat.2020.119156. Aug.

Bykov, G.L., Abkhalimov, E.V., Ershov, V.A., Ershov, B.G., 2022. Radiolysis of Portland cement and magnesium phosphate cement: effect of the content and state of water on the Physicochemical properties and the mechanism and kinetics of hydrogen formation. Radiat. Phys. Chem. 190, 109822. https://doi.org/10.1016/j.radphyschem.2021.109822. Jan.

Caes, S., Gurning, A.C., Li, X., de Souza, V., Kursten, B., 2023. Corrosion of aluminium in ordinary Portland cement paste: influence of matrix porosity and the presence of $LiNO_3$ corrosion inhibitor. Mater. Corros. 74 (1), 125–137. https://doi.org/10.1002/maco.202213296. Jan.

Cai, H., Liu, X., 1998. Freeze-thaw durability of concrete: ice formation process in pores. Cem Concr Res 28 (9), 1281–1287. https://doi.org/10.1016/S0008-8846(98)00103-3. Sep.

Chartier, D., et al., 2020. Behaviour of magnesium phosphate cement-based materials under gamma and alpha irradiation. J. Nucl. Mater. 541 (Dec). https://doi.org/10.1016/j.jnucmat.2020.152411.

Cheng, A., Chao, S.-J., Lin, W.-T., 2013. Effects of leaching behavior of calcium ions on compression and durability of cement-based materials with mineral admixtures. Materials 6 (5), 1851–1872. https://doi.org/10.3390/ma6051851. May.

Choi, Y.H., 2005. Nuclear waste management: gaining public acceptance. J. East Asian Aff. 19 (2), 225–261 [Online]. Available: http://www.jstor.org/stable/23257922.

Covill, A., Hyatt, N.C., Hill, J., Collier, N.C., 2011. Development of magnesium phosphate cements for encapsulation of radioactive waste. Adv. Appl. Ceram. 110 (3), 151–156. https://doi.org/10.1179/1743676110Y.0000000008. Apr.

Deltombe, E., Pourbaix, M., 1958. The electrochemical behavior of aluminum—potential pH diagram of the System AI-H2O at 25 °C. CORROSION 14 (11), 16–20. https://doi.org/10.5006/0010-9312-14.11.16. Nov.

During, E.D.D., 2018. Corrosion Atlas A Collection of Illustrated Case Histories THIRD. EXPANDED AND REVISED EDITION', Amersfoort.

Ekström, T., 2001. Leaching of Concrete : Experiments and Modelling. Division of Building Materials.

Electric Power Research Institute, 2006. 'Graphite decommissioning - options for graphite treatment. Recycling, or Disposal, including a discussion of Safety-Related Issues'.

Elkamash, A., Elnaggar, M., Eldessouky, M., 2006. Immobilization of cesium and strontium radionuclides in zeolite-cement blends. J. Hazard Mater. 136 (2), 310–316. https://doi.org/10.1016/j.jhazmat.2005.12.020. Aug.

Ente italiano di normazione, 2006. Manufatti di rifiuti radioattivi condizionati - Metodi di prova per la qualificazione dei processi di condizionamento per manufatti appartenenti alla Categoria 2 (UNI 11193:2006. Nov.

Ente italiano di normazione, 2016. 'Methods of Testing Cement - Part 1: Determination of Strength (UNI EN 196-1:2016)'. May 19.

Eskander, S.B., Bayoumi, T.A., Saleh, H.M., 2012. Performance of aged cement–polymer composite immobilizing borate waste simulates during flooding scenarios. J. Nucl. Mater. 420 (1), 175–181. https://doi.org/10.1016/j.jnucmat.2011.09.029.

European Commission Joint Research Centre, 2021. Technical Assessment of Nuclear Energy with Respect to the "Do No Significant Harm" Criteria of Regulation (EU) 2020/852 ("Taxonomy Regulation")'. Petten.

Fan, S., Chen, B., 2014. Experimental study of phosphate salts influencing properties of magnesium phosphate cement. Constr Build Mater 65, 480–486. https://doi.org/10.1016/j.conbuildmat.2014.05.021. Aug.

Fang, B., et al., 2023. Research progress on the properties and applications of magnesium phosphate cement. Ceram. Int. 49 (3), 4001–4016. https://doi.org/10.1016/j.ceramint.2022.11.078. Feb.

Galluccio, Francesco, Macerata, Elena, Mossini, Eros, Castagnola, Giovanni, Pierantoni, Veronica, Mariani, Mario, 2021. Recycling metal waste in nuclear decommissioning by advanced phosphoric acid decontamination process. Il Nuovo Cimento. https://doi.org/10.1393/ncc/i2020-20145-9. Mar.

Gardner, L.J., Bernal, S.A., Walling, S.A., Corkhill, C.L., Provis, J.L., Hyatt, N.C., 2015. Characterisation of magnesium potassium phosphate cements blended with fly ash and ground granulated blast furnace slag. Cem Concr Res 74, 78–87. https://doi.org/10.1016/j.cemconres.2015.01.015. Aug.

Godbee, H., Joy, D., 1974. Assessment of the Loss of Radioactive Isotopes from Waste Solids to the Environment. Part I. Background and Theory. https://doi.org/10.2172/4118334. Oak Ridge, TN (United States).

Gonzalez de Vicente, S.M., et al., 2022. Overview on the management of radioactive waste from fusion facilities: ITER, demonstration machines and power plants. Nucl. Fusion 62 (8), 085001. https://doi.org/10.1088/1741-4326/ac62f7. Aug.

Goo, J.-Y., Kim, B.-J., Kang, M., Jeong, J., Jo, H.Y., Kwon, J.-S., 2021. Leaching behavior of cesium, strontium, cobalt, and europium from immobilized cement matrix. Appl. Sci. 11 (18), 8418. https://doi.org/10.3390/app11188418. Sep.

Guo, J., Sun, W., Xu, Y., Lin, W., Jing, W., 2022. Damage mechanism and modeling of concrete in freeze–thaw cycles: a review. Buildings 12 (9), 1317. https://doi.org/10.3390/buildings12091317. Aug.

Hall, D.A., Stevens, R., El-Jazairi, B., 2001. The effect of retarders on the microstructure and mechanical properties of magnesia–phosphate cement mortar. Cem Concr Res 31 (3), 455–465. https://doi.org/10.1016/S0008-8846(00)00501-9. Mar.

Haque, M.A., Chen, B., 2019. Research progresses on magnesium phosphate cement: a review. Constr Build Mater 211, 885–898. https://doi.org/10.1016/j.conbuildmat.2019.03.304. Jun.

Hausner, H.H., 1963. Beryllium as a moderator and reflector for nuclear reactors. Vol: 1: No. 2. https://www.osti.gov/biblio/4708645.

Hinsenveld, M., 1991. Towards A New Approach in Modeling Leaching Behavior 331–340. https://doi.org/10.1016/S0166-1116(08)70417-5.

Hover, K.C., 2011. The influence of water on the performance of concrete. Constr Build Mater 25 (7), 3003–3013. https://doi.org/10.1016/j.conbuildmat.2011.01.010. Jul.

IAEA, 2017. 'INTERNATIONAL ATOMIC ENERGY AGENCY, Selection of Technical Solutions for the Management of Radioactive Waste, IAEA-TECDOC-1817'. Vienna.

IAEA, 2022a. 'INTERNATIONAL ATOMIC ENERGY AGENCY, Status and Trends in Spent Fuel and Radioactive Waste Management, IAEA Nuclear Energy Series No. NW-T-1.14 (Rev. 1)'. Vienna.

IAEA, 2022b. 'INTERNATIONAL ATOMIC ENERGY AGENCY, Communication and Stakeholder Involvement in Radioactive Waste Disposal, IAEA Nuclear Energy Series No. NW-T-1.16'. Vienna.

INTERNATIONAL ATOMIC ENERGY AGENCY, 1992. *Improved cement Solidification of Low and intermediate level radioactive wastes*, no. 350. In: Technical Reports Series. INTERNATIONAL ATOMIC ENERGY AGENCY, Vienna [Online]. Available: https://www.iaea.org/publications/1454/improved-cement-solidification-of-low-and-intermediate-level-radioactive-wastes.

INTERNATIONAL ATOMIC ENERGY AGENCY, 2007. New Developments and Improvements in Processing of 'Problematic' Radio Active Waste. INTERNATIONAL ATOMIC ENERGY AGENCY, Vienna [Online]. Available: https://www.iaea.org/publications/7815/new-developments-and-improvemen.

Ispettorato Nazionale per la Sicurezza Nucleare e la Radioprotezione, 2023. GUIDA TECNICA N. 33 - Criteri di sicurezza nucleare e radioprotezione per la gestione dei rifiuti radioattivi. Jan.

Khmurovska, Y., et al., 2021. Effects of gamma-ray irradiation on hardened cement mortar. Int J Concr Struct Mater 15 (1), 17. https://doi.org/10.1186/s40069-020-00452-7. Dec.

Kim, Y.S., Chae, H.T., Van den Berghe, S., Leenaers, A., Kuzminov, V., Yacout, A.M., 2020. Aluminum cladding oxide growth prediction for high flux research reactors. J. Nucl. Mater. 529, 151926. https://doi.org/10.1016/j.jnucmat.2019.151926. Feb.

Lahalle, H., et al., 2016. Investigation of magnesium phosphate cement hydration in diluted suspension and its retardation by boric acid. Cem Concr Res 87, 77–86. https://doi.org/10.1016/j.cemconres.2016.04.010. Sep.

Lahalle, H., Patapy, C., Glid, M., Renaudin, G., Cyr, M., 2019. Microstructural evolution/durability of magnesium phosphate cement paste over time in neutral and basic environments. Cem Concr Res 122, 42–58. https://doi.org/10.1016/j.cemconres.2019.04.011. Aug.

Le Rouzic, M., Chaussadent, T., Platret, G., Stefan, L., 2017. Mechanisms of k-struvite formation in magnesium phosphate cements. Cem Concr Res 91, 117–122. https://doi.org/10.1016/j.cemconres.2016.11.008. Jan.

Li, Y., Chen, B., 2013. Factors that affect the properties of magnesium phosphate cement. Constr Build Mater 47, 977–983. https://doi.org/10.1016/j.conbuildmat.2013.05.103. Oct.

Luhar, I., et al., 2023. Solidification/stabilization technology for radioactive wastes using cement: an appraisal. Materials 16 (3), 954. https://doi.org/10.3390/ma16030954. Jan.

Macfarlane, A.M., 2011. The overlooked back end of the nuclear fuel cycle. Science (1979) 333 (6047), 1225–1226. https://doi.org/10.1126/science.1207054. Sep.

Marsal, F., et al., 2023. EURAD EC project – overview of the routes work package: identified key issues and open questions about waste management routes in Europe, from cradle to grave. EPJ Nuclear Sciences & Technologies 9, 1. https://doi.org/10.1051/epjn/2022024. Jan.

Mendibide, C., Dusquesnes, V., Deydier, V., Bourbon, X., Crusset, D., 2021. Corrosion behavior of aluminum alloy 5754 in cement-based matrix-simulating nuclear waste disposal conditions. Mater. Corros. 72 (1–2), 383–395. https://doi.org/10.1002/maco.202011687. Jan.

Moschetti, I., Sarrasin, L., Blain, G., Mossini, E., Mariani, M., Abdelouas, A., 2023. Effect of curing time and water to binder ratio on magnesium potassium phosphate cement exposed to gamma irradiation. In: ASME 2023 International Conference on Environmental Remediation and Radioactive Waste Management. American Society of Mechanical Engineers. https://doi.org/10.1115/ICEM2023-109457. Oct.

Mossini, E., et al., 2023. Pre-impregnation approach to encapsulate radioactive liquid organic waste in geopolymer. J. Nucl. Mater. 585, 154608. https://doi.org/10.1016/j.jnucmat.2023.154608. Nov.

Nuclear Energy Agency, 2015. 'Nuclear Energy: Combating Climate Change'. Paris.

Ojovan, M.I., Lee, W.E., 2014. An introduction to nuclear waste immobilisation. In: An Introduction to Nuclear Waste Immobilisation. Elsevier. https://doi.org/10.1016/B978-0-08-099392-8.00001-2.

Ojovan, M.I., Varlackova, G.A., Golubeva, Z.I., Burlaka, O.N., 2011. Long-term field and laboratory leaching tests of cemented radioactive wastes. J. Hazard Mater. 187 (1–3), 296–302. https://doi.org/10.1016/j.jhazmat.2011.01.004. Mar.

Park, J.W., Kim, K.H., Ann, K.Y., 2016. Fundamental properties of magnesium phosphate cement mortar for rapid repair of concrete. Adv. Mater. Sci. Eng. 2016, 1–7. https://doi.org/10.1155/2016/7179403.

Penttala, V., Al-Neshawy, F., 2002. Stress and strain state of concrete during freezing and thawing cycles. Cem Concr Res 32 (9), 1407–1420. https://doi.org/10.1016/S0008-8846(02)00785-8. Sep.

Pyo, J.-Y., Um, W., Heo, J., 2021. Magnesium potassium phosphate cements to immobilize radioactive concrete wastes generated by decommissioning of nuclear power plants. Nucl. Eng. Technol. 53 (7), 2261–2267. https://doi.org/10.1016/j.net.2021.01.005. Jul.

Qin, Z., Ma, C., Zheng, Z., Long, G., Chen, B., 2020. Effects of metakaolin on properties and microstructure of magnesium phosphate cement. Constr Build Mater 234, 117353. https://doi.org/10.1016/j.conbuildmat.2019.117353. Feb.

Rivonkar, A., et al., 2022. Optimisation of the chemical oxidation reduction process (CORD) on surrogate stainless steel in regards to its efficiency and secondary wastes. Frontiers in Nuclear Engineering 1. https://doi.org/10.3389/fnuen.2022.1080954. Dec.

Robertson, D.E., Thomas, C.W., Wynhoff, N.L., Hetzer, D.C., 1990. Characterization of long-lived activation products in spent fuel assembly hardware and reactor pressure vessel steel. Nucl. Eng. Des. 118 (3), 463–486. https://doi.org/10.1016/0029-5493(90)90047-2. Apr.

Saha, A.K., 2018. Effect of class F fly ash on the durability properties of concrete. Sustainable Environment Research 28 (1), 25–31. https://doi.org/10.1016/j.serj.2017.09.001. Jan.

Saleh, H., Eskander, S., 2013. Solidification of hot real radioactive liquid scintillator waste using cement-clay composite. Monatshefte fuer Chemie/Chemical Monthly 144, 1751–1758. https://doi.org/10.1007/s00706-013-1065-9. Sep.

Saleh, H.M., Bondouk, I.I., Salama, E., Mahmoud, H.H., Omar, K., Esawii, H.A., 2022. Asphaltene or polyvinylchloride waste blended with cement to produce a sustainable material used in nuclear safety. Sustainability 14 (6). https://doi.org/10.3390/su14063525.

Santi, A., et al., 2022. Design of sustainable geopolymeric matrices for encapsulation of treated radioactive solid organic waste. Front Mater 9 (Oct). https://doi.org/10.3389/fmats.2022.1005864.

Setiadi, A., Milestone, N.B., Hill, J., Hayes, M., 2006. Corrosion of aluminium and magnesium in BFS composite cements. Adv. Appl. Ceram. 105 (4), 191–196. https://doi.org/10.1179/174367606X120142. Aug.

Shon, J.S., Kim, G.Y., Im, J., 2019. Evaluation of efficient cementation of fission 99Mo production process waste and feasibility disposal of cement waste form. Ann. Nucl. Energy 124, 342–348. https://doi.org/10.1016/j.anucene.2018.09.029. Feb.

Shon, J.-S., Lee, H.-K., Kim, T.-J., Kim, G.-Y., Jeon, H., 2022. Evaluation of cementation of intermediate level liquid waste produced from fission 99Mo production process and disposal feasibility of cement waste form. Nucl. Eng. Technol. 54 (9), 3235–3241. https://doi.org/10.1016/j.net.2022.03.033. Sep.

Takada, M., et al., 2022. Important factors for public acceptance of the final disposal of contaminated soil and wastes resulting from the Fukushima Daiichi nuclear power station accident. PLoS One 17 (6), e0269702. https://doi.org/10.1371/journal.pone.0269702. Jun.

Thomson, M., Lindqvist, J., Elsen, J., Groot, C., 2007. Chapter 2.5 Characterisation: Porosity of Mortars. ', p. 75.

van der Laan, J.G., Fedorov, A.V., van Til, S., Reimann, J., 2012. Ceramic breeder materials. In: Comprehensive Nuclear Materials. Elsevier, pp. 463–510. https://doi.org/10.1016/B978-0-08-056033-5.00114-2.

Vinokurov, S.E., Kulyako, Yu M., Slyuntchev, O.M., Rovny, S.I., Myasoedov, B.F., 2009. Low-temperature immobilization of actinides and other components of high-level waste in magnesium potassium phosphate matrices. J. Nucl. Mater. 385 (1), 189–192. https://doi.org/10.1016/j.jnucmat.2008.09.053. Mar.

Wagh, A.S., et al., 2016. Experimental study on cesium immobilization in struvite structures. J. Hazard Mater. 302, 241–249. https://doi.org/10.1016/j.jhazmat.2015.09.049. Jan.

Walling, S.A., Provis, J.L., 2016. Magnesia-based cements: a journey of 150 Years, and cements for the future? Chem Rev 116 (7), 4170–4204. https://doi.org/10.1021/acs.chemrev.5b00463. Apr.

Wang, S., Song, S., Huang, M., Xie, Z., Zhang, L., Zheng, W., 2022. Effect of water immersion on compressive properties of coir fiber magnesium phosphate cement. Polymers 14 (24), 5339. https://doi.org/10.3390/polym14245339. Dec.

Xu, B., Ma, H., Shao, H., Li, Z., Lothenbach, B., 2017. Influence of fly ash on compressive strength and micro-characteristics of magnesium potassium phosphate cement mortars. Cem Concr Res 99, 86–94. https://doi.org/10.1016/j.cemconres.2017.05.008. Sep.

Yu, B., Zhou, J., Cheng, B., Yang, W., 2021. Compressive strength development and microstructure of magnesium phosphate cement concrete. Constr Build Mater 283, 122585. https://doi.org/10.1016/j.conbuildmat.2021.122585. May.